C. FAELLA
Dipartimento di Ingegneria Civile, Università di Salerno
E. MARTINELLI
Dipartimento di Ingegneria Civile, Università di Salerno
E. NIGRO
Dipartimento di Analisi e Progettazione Strutturale, Università di Napoli "Federico II"

INTERMEDIATE DEBONDING IN FRP STRENGTHENED RC BEAMS: A NUMERICAL MODEL

Abstract

One of the most effective ways for improving the flexural strength of RC members consists in bonding FRP laminates at their soffit in order to upgrade the existing tensile strength. Strengthening RC beams by Externally Bonded FRP laminates is getting more and more common and various Codes of Standards have been issued in Europe, United States and Japan. In particular, the most up-to-date document has been released in Italy one year ago.

A key problem to be faced when managing FRP strengthened beams deals with the possible premature failure due to debonding between the adhesive layer and concrete, which can occur at the beam end (end debonding) or in the cracked zone (intermediate debonding).

In the present paper, a mechanical model considering non-linear stress-strain relationships for concrete, steel and FRP-to-concrete interface is presented, with the aim of simulating the behavior of RC beams strengthened by externally bonded FRP plates.

1. INTRODUCTION

In the last years huge research efforts have been carried out for understanding the behavior of reinforced concrete beams strengthened by externally bonded FRP. The main subject of these studies is the mechanical characterization of the FRP-to-concrete adhesive interface.

Different contributions about this topic have been summarized and compared in Chen & Al. (2001). Roberts (1988) provided a simplified model for evaluating interface stresses in FRP (or even steel) strengthened beams; simplified equations for evaluating shear and normal stresses throughout the FRP-to-concrete interface have been provided by assuming linear elastic behavior of the adhesive interface. Similar relationships, even obtained under simplified hypotheses for the interface behavior, have been provided in Malek & Al. (1998); the authors showed, even through experimental and numerical comparisons, that such simplified formulae usually result in a close approximation of the complex stress patterns which develop throughout the FRP-to-concrete interface.

The above mentioned papers mainly deal with interface stress distribution in the elastic range, which is an aspect of concern for serviceability conditions. Premature loss of bonding between FRP and concrete needs to be studied by considering a suitable non-linear relationship between interface stresses and strains. Holzenkaempfer (1994) proposed a bi-linear relationship between shear stresses and interface slips; based on such model, Taljsten (1997) determined the expressions of the ultimate bearing capacity of FRP-to-concrete joints.

Further studies have been devoted to end and intermediate debonding occurrence, but nowadays definitive solutions have not yet reached. Nevertheless, various proposals have been derived from simplified mechanical models and calibrated making use of the experimental results available in the scientific literature (Teng & Al., 2002).

Some of the findings of these studies have been also utilized in the following Code of Standards issued in various countries:

- fib bulletin 14 (2001) in Europe;
- ACI 440 (2002) in the United States;
- JSCE Recommendations (2001) in Japan;
- Italian Code CNR DT 200 (2004).

In the present paper, a numerical model is firstly presented for simulating the behavior of reinforced concrete beams externally bonded by FRP materials. The model is based on a similar one proposed by the authors for steel-concrete composite beams ac-

cording to the well-known Newmark approach (Newmark & Al., 1951) which considers two Bernoulli beams connected by means of a linear behaving interface. Interface slips between reinforced concrete beam and FRP plate or fabric are considered and, consequently, a well-established non-linear shear stress-slip law is introduced. Moreover, non-linear stress-strain relationships are utilized for modeling the other structural materials and a completely non-linear analysis procedure is obtained by means of a secant approach; such non-linear procedure allows reproducing the whole structural behavior up to failure which can be due to FRP tearing, concrete crushing or interface debonding. The present study is mainly focused on debonding failure which can occur at the FRP-cut-off section (end debonding) or throughout the FRP-to-concrete adhesive interface (intermediate debonding).

2. THE THEORETICAL MODEL

In the present section an analytical model is presented for simulating the composite behavior of FRP-strengthened RC beams. On the basis of such a model, the formulation of a finite element is presented and a secant procedure for non-linear analysis is also described.

2.1 Analytical formulation

A theoretical model can be formulated for simulating the mechanical behavior of reinforced concrete beams externally strengthened by means of FRP materials. The following assumptions are made:

- the RC beam behaves to the Bernoulli theory, while FRP plate flexural stiffness is neglected and only axial forces are considered;
- the interaction between the two members is realized through a continuous, linear behaving and thicknessless medium;
- equal transverse displacements, i.e. deflections, occur in the connected members.

The partial interaction between beam and FRP results in an interface slip s which can be expressed as follows if the above hypotheses apply:

$$s = u_{f,sup} - u_{c,inf} = u_f - \varphi \cdot y_{f,sup} - (u_c + \varphi \cdot y_{c,inf}) = u_f - u_c - \varphi \cdot d \quad (1)$$

with the symbol reported in Fig. 1 and $y_{f,sup} = t_f/2$; in particular d is the distance between beam and FRP plate centroids. However, assuming $F_f = -F_c = F$, it results:

$$M = \chi \cdot EI_c + F \cdot d \quad (2)$$

where χ is the curvature and EI_c is the flexural stiffness of RC beam cross section without considering FRP.

The longitudinal shear force per unit length F^l depends linearly on the interface slip s:

$$F^l = k \cdot s = k_a b_f \cdot s \quad (3)$$

k being the stiffness constant which characterizes the shear connection; it can be obtained by multiplying the adhesive slip modulus (namely, transverse stiffness) k_a and the width b_f of the adhesive layer.

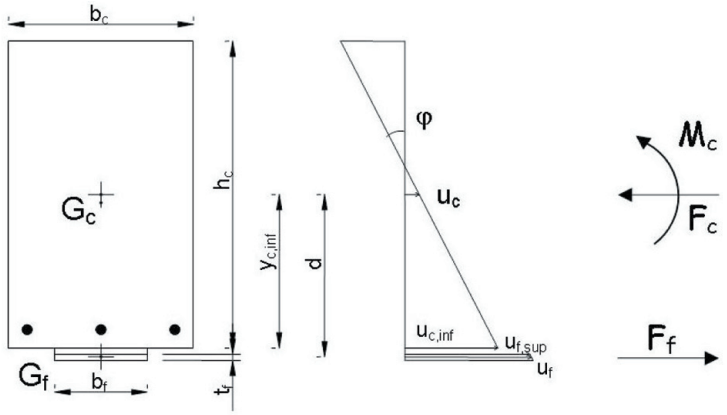

Fig. 1: Transverse section of FRP-strengthened RC beam.

Using the compatibility equation (1), the equilibrium equation (2) and the interface relationship (3), the following second-order differential equation in terms of curvature may be obtained:

$$\chi'' - \alpha^2 \chi = -\alpha^2 \frac{M}{EI_{full}} - \frac{q}{EI_c} \qquad (4)$$

where EI_{full} represents the flexural stiffness of the overall cross-section when no interface slips occur and can be defined as follows if the above mentioned hypotheses apply:

$$EI_{full} = EI_c + \frac{E_f A_f \cdot EA_c}{E_f A_f + EA_c} \cdot d^2 = EI_c + EA^* \cdot d^2 \qquad (5)$$

The parameter α in equation (4) is defined as follows:

$$\alpha^2 = \frac{k}{EA^*} \cdot \frac{EI_{full}}{EI_c} \qquad (6)$$

being k the slip modulus of the FRP-to-concrete adhesive interface.

The equations briefly outlined above could even be obtained by simplifying the equation formulated within the well-known Newmark theory, widely utilized for steel-concrete composite beams, and neglecting the flexural stiffness of the bottom element connected to RC beam.

2.2 Outlines of the finite element formulation

A finite element can be formulated (among the other possible choices) implementing the exact solution of the structural problem for carrying out linear analyses of RC beams externally strengthened by FRP plates. According to the mentioned approach a formally "force based" finite element can be derived by directly solving equation (4) in order to obtain the various terms of the

flexibility matrix **D** and the vector δ_0 of nodal displacements due to distributed loads. The usual relationship of flexibility-based finite elements can be obtained for the simply supported FRP-strengthened beam element:

$$\ddot{\mathbf{a}} = \mathbf{D}\mathbf{X} + \ddot{\mathbf{a}}_0 \qquad (7)$$

X and δ being the vectors of nodal forces and displacements, respectively, whose four components are represented in Fig. 2a.

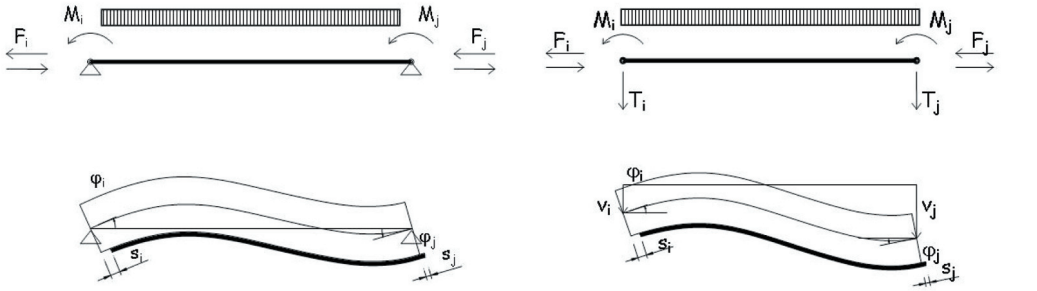

a) simply supported-beam for force based element; *b) unrestrained beam for displacement-based element*

Fig. 2: Nodal force and displacement components.

The usual displacement-based relationship which relates nodal forces and displacement for the unrestrained FRP-strengthened beam (Fig. 2b) can be obtained by inverting the flexibility matrix and completing it with nodal shear forces as explained in Faella & Al. (2002). The usual relationship between nodal force vectors **Q**, $\mathbf{Q}_0$, and nodal displacement vectors **s** (both characterized by the six components represented in Fig. 2b) can be written as follows by means of the stiffness matrix **K**:

$$\mathbf{Q} = \mathbf{K}\mathbf{s} + \mathbf{Q}_0 \qquad (8)$$

2.3 Details about the non-linear numerical procedure

Non linear behavior of the materials constituting the FRP strengthened RC beams can be easily introduced by means of fiber discretization of the beam cross section and a secant approach.

Three non-linear phenomena have to be considered for simulating the premature failure possibly due to FRP-to-concrete debonding which can occur in an intermediate section or at the FRP cut-off section. The first one deals with the overall behavior of concrete in compression and tension; the rational formula proposed by Saenz is adopted for concrete in compression while a simple linear relationship up to the tensile stress value is considered for concrete in tension (Fig. 3).

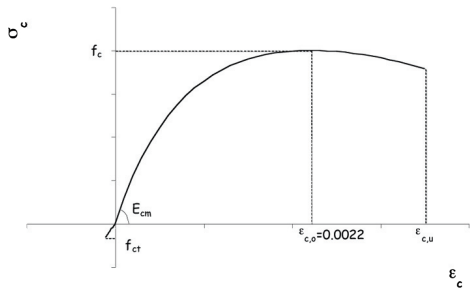

Fig. 3. Non-linear stress-strain law for concrete.

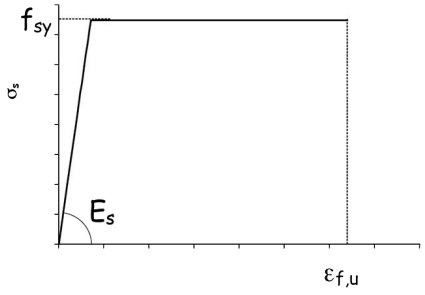

Fig. 4. Stress-strain law for rebar steel.

Moreover, accounting for yielding in steel rebars is essential for modeling intermediate debonding phenomena in FRP-strengthened beams; the typical stress-strain relationship for steel rebars is represented in fig. 4 and will be adopted in the numerical analyses. Strain-hardening in steel is actually neglected (even if it would be very easy to be introduced in the model) because strain values in FRP-strengthened beams are usually not so great for strain hardening to be developed in steel rebars.

The well-established and widely accepted elastic-brittle stress-strain relationship is assumed for FRP plate (Fig. 5).

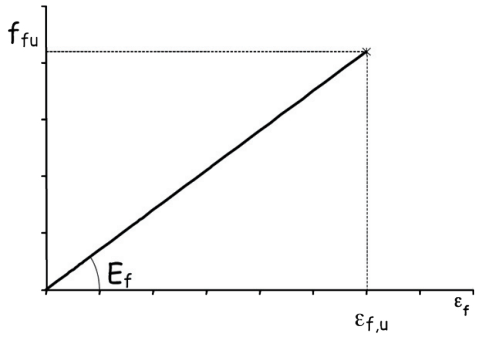

Fig. 5. Elastic-brittle stress-strain relationship for FRP plate.

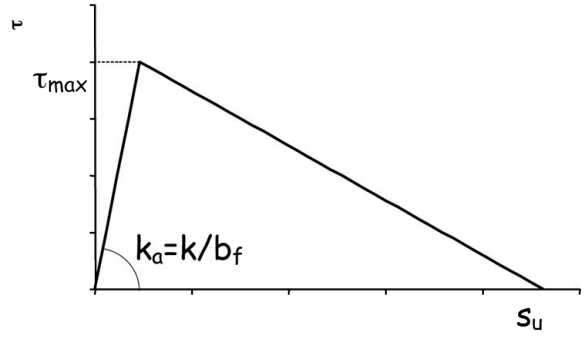

Fig. 6. Bi-linear shear stress-interface slip relationshipeterface.

Finally, shear behavior of the adhesive interface connecting FRP laminate or fabric to the soffit of the beam can be described by means of the well-known bi-linear elastic-softening curve (fig. 6) introduced by Holzenkaempfer (1994). The linear branch of the interface law is characterized by the shear stiffness $k_a=k/b_f$ which can be related to the slip modulus k introduced in eq. (2).

Fiber discretization (Fig. 7) is considered for cross section in order to evaluate the secant stiffnesses of reinforced concrete section and the slip modulus of the adhesive interface.

The given FRP-strengthened beam is subdivided in n elements throughout its axis and, in correspondence of the i-th load step, the j-th element is characterized by the initial values of stiffness with reference to the beam cross section $EI_{c,j}^{(i,0)}$ and $EA_{c,j}^{(i,0)}$, the adhe-

sive interface $k_j^{(i,0)}$, and the current value of the centroidal distance $d^{(i,0)}$ between FRP plate and the effective RC section. Therefore, for the i-th load step an iterative procedure must be carried out in order to determine the corresponding vector $\mathbf{s}^{(i)}$ of nodal displacements; at the k-th iteration, the secant stiffness matrix obtained considering the secant values $EI_{c,j}^{(i,k)}$, $EA_{c,j}^{(i,k)}$ and $k_j^{(i,k)}$ of the elements can be obtained and the corresponding displacements $\mathbf{s}^{(i,k)}$ can be determined:

$$\mathbf{K}^{(i,k)}\mathbf{s}^{(i,k)} = \mathbf{Q}^{(i)} - \mathbf{Q}_0^{(i,k)} \tag{9}$$

being $\mathbf{Q}^{(i)}$ the nodal forces at the i-th load step (independent by the current values of element stiffnesses) and $\mathbf{Q}_0^{(i,k)}$ the nodal forces equivalent to the external actions considered at the same i-th load level and determined with reference to the k-th values of the element secant stiffness. On the bases of the nodal displacements obtained by (9) the slip modulus k_j is updated to obtain the corresponding secant stiffness $k_j^{(i,k+1)}$ depending upon the shear-stress-relative-slip relationship assumed in the analysis and generically represented in fig. 6. Moreover, the secant flexural stiffness can be evaluated for each element at the end of the k-th iteration by considering the current bending moment $M_j^{(i,k)}$ and axial force $N_j^{(i,k)}$. Given the current values of axial strain $\varepsilon_{c,j}^{(i,k)}$ and curvature $\chi_j^{(i,k)}$ of the section, fiber discretization (Fig. 7) of the beam cross section allows to determine the corresponding values of the resulting internal bending moment $M_{c,j}^{(i,k)}$ and axial force $N_{c,j}^{(i,k)}$ obtained by considering the stress-strain relationships which describe concrete and steel behavior. Consequently, the updated values of the beam stiffnesses can be determined as follows

$$EA_{c,j}^{(i,k+1)} = \frac{N_{res,j}^{(i,k)}}{\varepsilon_{c,j}^{(i,k)}}, \quad EI_{c,j}^{(i,k+1)} = \frac{M_{res,j}^{(i,k)}}{\chi_j^{(i,k)}}. \tag{10}$$

as well as the distance $d_j^{(i,k+1)}$ can be determined by considering the

distance between the effective section of the reinforced concrete beams and the FRP plate.

$$\varepsilon_{c,j}^{(i,k)} = \frac{N_j^{(i,k)}}{EA_{c,j}^{(i,k)}} \quad \chi_{c,j}^{(i,k)} = \frac{M_j^{(i,k)}}{EI_{c,j}^{(i,k)}} \tag{11}$$

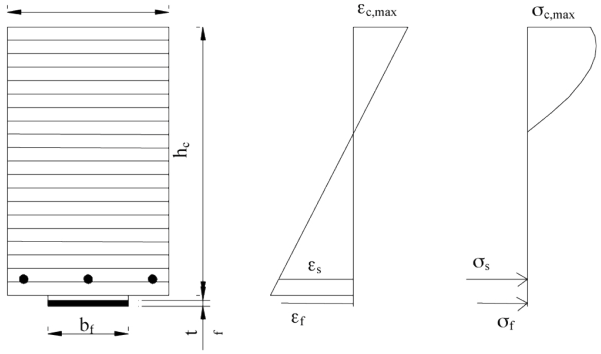

Fig. 7. Cross section of the FRP-strengthened beam: relevant dimensions and fiber discretization of the reinforced concrete portion.

Finally, all the stiffness parameters needed for defining the element secant stiffness matrix $\mathbf{K}^{(i,k+1)}$ and the vector of equivalent nodal forces $\mathbf{Q}^{(i,k+1)}$ can be now determined on the bases of eqs. (5)-(7). Convergence under the i-th load step is reached as the difference between nodal displacements determined after k-th and the (k+1)-th iteration are lesser than a given threshold value Δ:

$$\left| \mathbf{s}^{(i,k+1)} - \mathbf{s}^{(i,k)} \right| < \Delta \tag{12}$$

The analysis can be generally pursued until one of the following failure modes is attained:

- concrete crushing, which occurs if the maximum value ε_c measured on the concrete fibers at the convergence of the i-th load step achieves its ultimate value ε_{cu};
- steel rupture, occurring if the steel tensile strain ε_s reaches

the correspondent limit value ε_{su};

- FRP plate tearing, whose occurrence is pointed out if the fiber axial strain ε_f measured in FRP at convergence of the i-th load step achieves its ultimate value ε_{fu};
- FRP debonding, depending on the fact that the maximum interface slip reaches the ultimate value considered in the shear-stress-interface-slip relationship assumed in the analysis.

Therefore, the proposed model is able to determine the whole behavior of RC beams externally strengthened by FRP plates. In particular, the following sections are mainly devoted to understand the debonding failure mode which can occur in FRP-strengthened RC beams. The analyses that will be proposed are basically aimed to obtain the value of the external loads which results in debonding failure and the corresponding maximum value of the axial strain developed in FRP.

3 VALIDATION OF THE NUMERICAL MODEL

The current section is devoted to show how the numerical model formulated in the previous one is able to simulate the behavior of the FRP-strengthened beams and their failure mode.
Therefore, a large database of about 30 experimental cases of observed intermediate debonding failures, listed in the reference section, have been collected to assess the accuracy of the numerical procedure. The non-linear stress-strain laws introduced in the previous section are assumed for concrete and steel bars, while elastic-brittle behavior is considered for FRP. The adhesive interface is modeled by means of the above mentioned bi-linear relationship, whose characteristic parameters are determined according to the fib bulletin 14 – approach 2 proposal reported in the following:

$$\tau_{max} = 0.285 \cdot \sqrt{f_{ck} \cdot f_{ctm}} \text{ [MPa]} \qquad (13)$$

$s_u = 0.185$ [mm].	(14)

The elastic branch of the stress-slip relationship is assumed by considering the shear stiffness of the adhesive layer looking after the possible contribution of the concrete cover in terms of flexibility as explained in [0].

Fig. 8 to Fig. 9 show various cases of simply supported beams externally strengthened by FRP and demonstrates how in both cases the complete evolution of the displacement-vs-force curve can be followed by the numerical procedure which provides also a good estimation of the ultimate load and displacement. In particular, the former one is always reproduced with great accuracy by the numerical simulation, while the latter is sometimes affected by some errors with respect to the experimental one due to the small load gradient at collapse and the direct dependence of the ultimate displacement on the ultimate slip value s_u: due to the lack of information about interface fracture energy provided by the authors of the experiments, it has been assumed on the bases of the *fib* proposal (14).

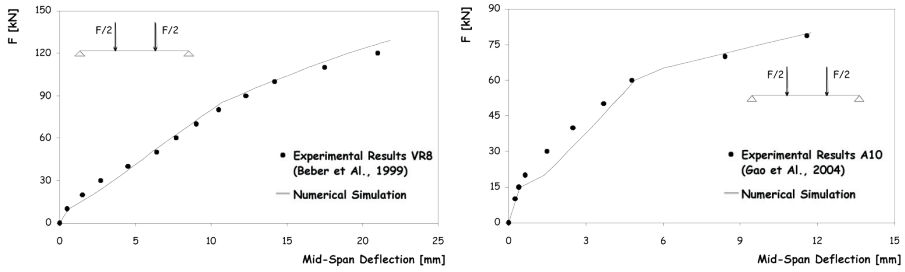

Fig. 8. Experimental comparison on simply supported beams: Load-Deflection curves.

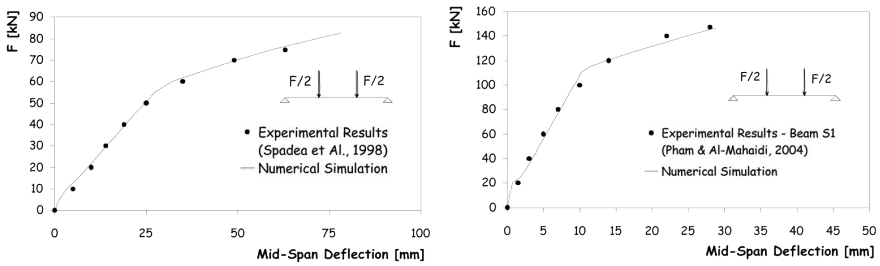

Fig. 9. Experimental comparison on simply supported beams: Load-Deflection curves.

Fig. 10 is devoted to another of the experimental cases which have been found in the scientific literature; a cantilever beam externally strengthened by FRP is reported in that work and the main results in terms of load-deflection curve are represented in Fig. 11 demonstrating once more that the numerical procedure is able to reproduce the observed behavior resulting in a very refined evaluation of the ultimate load and deflection at debonding.

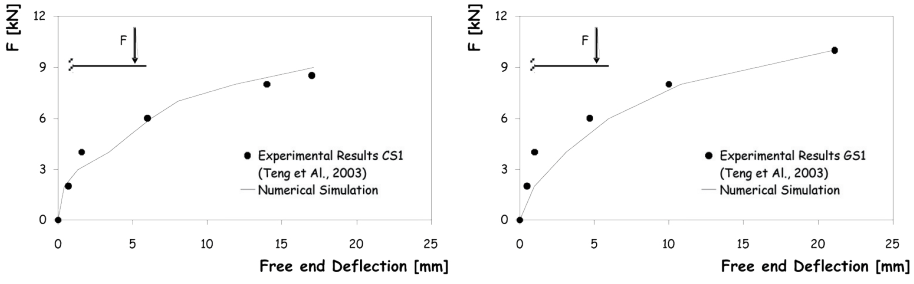

Fig. 10. Experimental comparison cantilever beams: Load-Deflection curves.

The load deflection curves obtained for the other experimental cases which have been taken from the scientific literature are not represented in the present paper for the sake of brevity. Nevertheless, a wider experimental-to-numerical comparison at a glance in terms of force, maximum beam deflection and maximum FRP axial strain is represented in Fig. 11, Fig. 12 and Fig. 13, respectively.

Quite remarkable accuracy is shown in all the three quoted figures which compare the experimentally measured parameters and the results of the numerical analyses. It is worth to precise that all the average values of the mechanical properties have been adopted in the numerical analyses when provided by the authors; well-established relationships have been utilized sometimes to integrate the mechanical properties when not completely reported in the original papers..

Fig. 11 shows the complete comparison between experimental results and numerical simulation in terms of the maximum beam load resulting in debonding; a substantial equivalence can be observed between the experimental and numerical values even if they span in a very wide range due to the fact that various structural schemes, different geometric characteristics and mechanical properties have been considered in the database.

The same accuracy can be observed in Fig. 12 where the experimental-to-numerical comparison is presented in terms of beam deflections with reference to the same cases considered above.

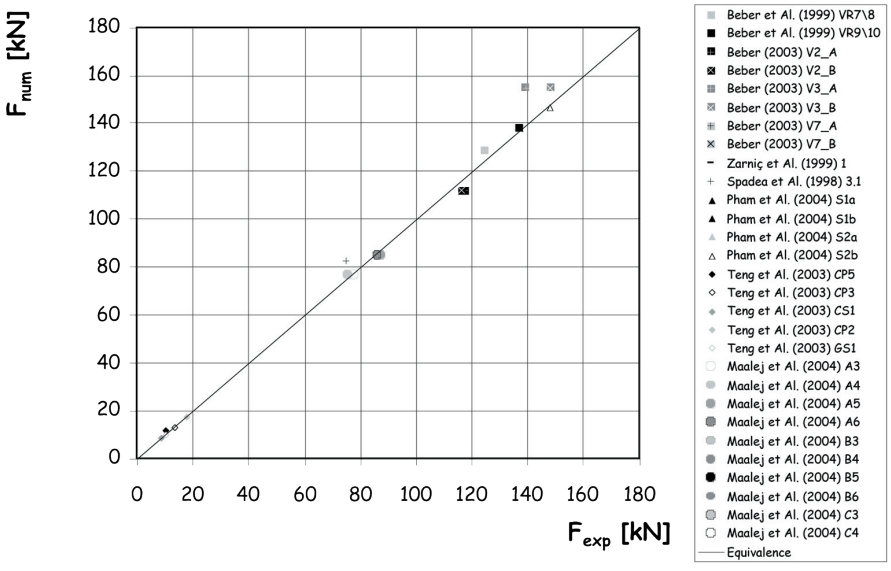

Fig. 11. Experimental vs Numerical comparison in terms of maximum load at debonding.

Finally, Fig. 13 shows FRP maximum strain at debonding, ε_f, which is one of the most important parameter considered in various code provisions (i.e., ACI 440, fib bulletin 14 – approach 1, and CNR Italian Recommendations) in order to assess the ultimate flexural resistance of the FRP-strengthened beam. In fact premature beam flexural collapse may occur due to debonding failure which does not allow developing FRP strain up to its tearing rupture. Also in this case the accuracy can be deemed satisfactory, even if the distance between some points and the equivalence line is more scattered than in either fig. 12 and fig. 13, due to the fact that FRP strain is directly affected by some local phenomena and mechanical properties (such as concrete tensile strength and interface bond) which can be different throughout the beam axis. Consequently, the numerical procedure formulated in the present paper can be effectively utilized for simulating the behavior of FRP-strengthened beams.

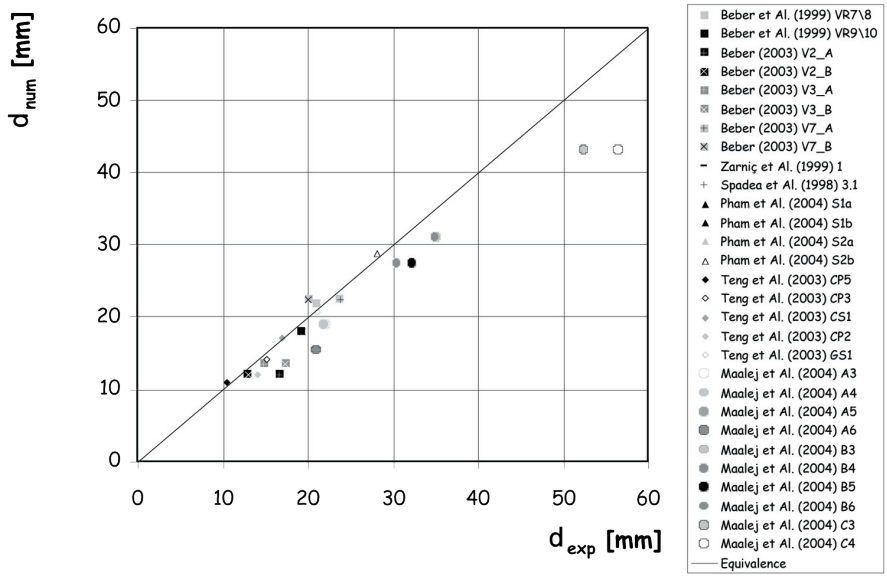

Fig. 12. Experimental vs Numerical comparison in terms of beam maximum displacement at debonding.

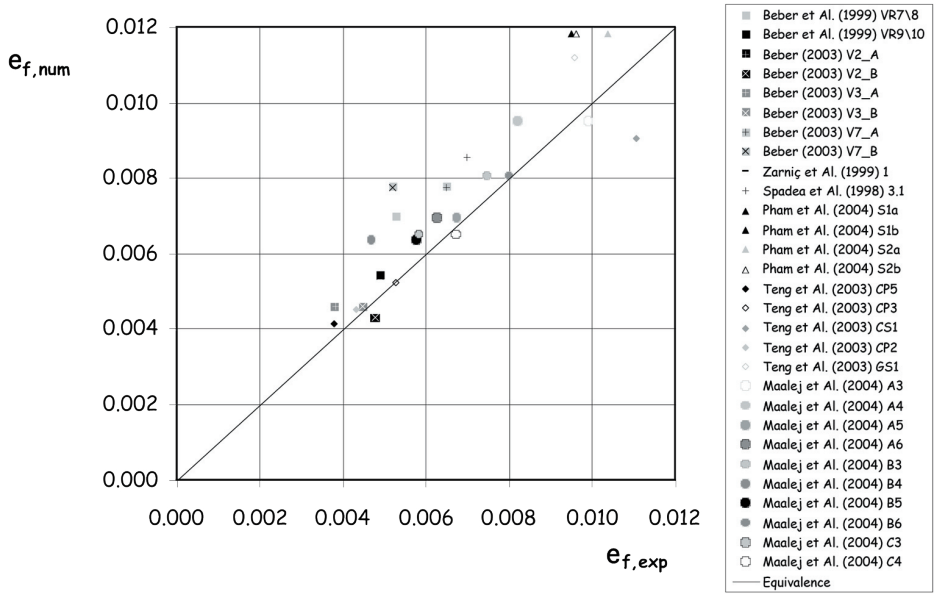

Fig. 13. Experimental vs Numerical comparison in terms of FRP strain at debonding.

4 DEBONDING FAILURE: THE KEY PARAMETERS

The numerical procedure presented in the previous sections has been utilized for carrying out a very wide parametric analysis to exploring the significant cases of RC beams strengthened by externally bonded FRP plates or fabrics. The following parameters and the corresponding ranges have been considered:

- concrete compressive strength f_{ck} , which controls both the concrete stress-strain relationship and the shear stress-interface slip law. The relationships assumed for characterizing these two (generalized) stress-strain laws can be taken from the mentioned companion paper. With the aim of covering a significant parametric field, the value of f_{ck} ranges between 20 and 40 MPa;
- rebar steel yielding stress f_{sy} , which plays a key role in affecting the intermediate debonding failure; it has been taken between 215 and 375 MPa, that can be usually found

in members of existing RC structures;

- FRP Young Modulus E_f , which has been assumed to range between 140000 and 220000 MPa, covering all the field of carbon fiber plates and fabrics usually more utilized in flexural strengthening than glass fiber materials;
- beam cross section height h, which ranges between 250 and 500 mm, as usual for common beams and slabs in ordinary buildings;
- FRP plate section, whose values have been assumed on the bases of the current value of the beams cross-section area A_c, ranging between 0.0005 A_c and 0.0015 A_c;
- FRP plate width b_f, which ranged between 75 and 125 mm;
- steel rebar area , whose values have been assumed on the bases of the current value of the beams cross section area A_c , ranging between 0.0015 A_c and 0.015 A_c;
- beam span length , ranging between 3000 and 7000 mm.

The maximum FRP strain $\varepsilon_{f,max}$ attained throughout the beam under the ultimate load as been regarded for determining if whether or not premature failure occurs. In particular, intermediate debonding failure occurs if $\varepsilon_{f,max}$ is less than the FRP ultimate tensile strain $\varepsilon_{f,u}$.

A substantially decreasing trend can be observed in FRP axial strain $\varepsilon_{f,max}$ with respect to its specific axial stiffness $E_f t_f$. ACI 440 provisions are basically founded on this correlation between $\varepsilon_{f,max}$ and $E_f t_f$, whatever be the other beam and FRP properties, in particular those concerning with the FRP-to-concrete adhesion, which plays a direct role in controlling debonding crisis (Fig. 14).

The same points represented in Fig. 14 are also reported in Fig. 15 by distinguishing the various them in terms of the energy fracture G_f adopted in the analyses. Three bundles can be observed in the figure, each one characterized by a dispersion lesser than the one of the complete series of data; in particular, as expected, the higher is the fracture energy value, the greater becomes the FRP strain developed in FRP at debonding.

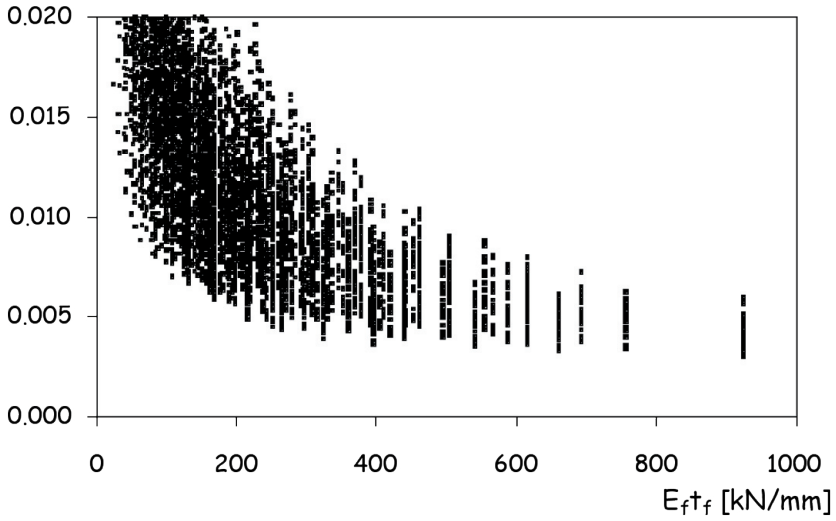

Fig. 14. Maximum FRP strain at debonding vs FRP specific axial stiffness.

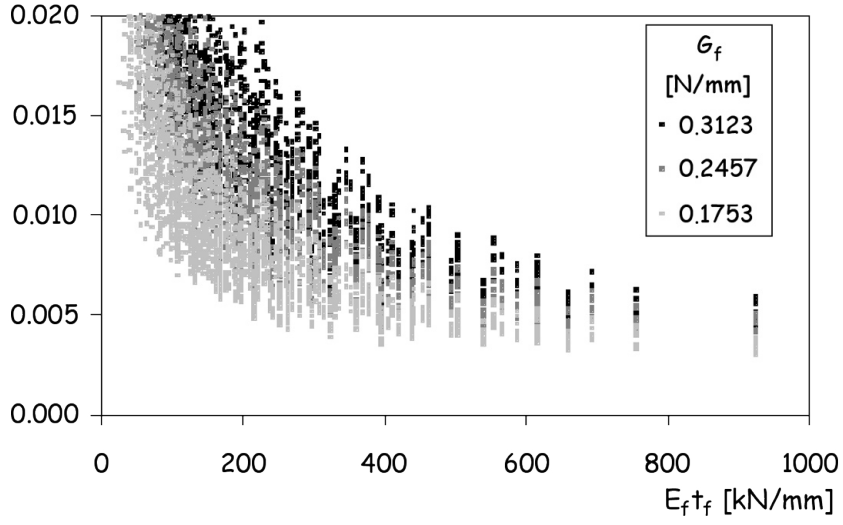

Fig. 15. Maximum FRP strain at debonding vs FRP specific axial stiffness: the role of fracture energy.

Therefore, the previous figures pointed out the relationship between two parameters (namely, $E_f t_f$ and $E_f t_f/2G_f$) which are already considered in some simplified formulae.

The role of further parameters can be emphasized making use of the results of the parametric analysis.

In Fig. 16 three boundless characterized by different ranges of steel mechanical ratio ω_s have been represented. The average curves drawn to put in evidence the trend of variation of each bundle with respect to the parameter reported on the x-axis show that the FRP maximum strain at debonding increases as the steel mechanical ratio decreases.

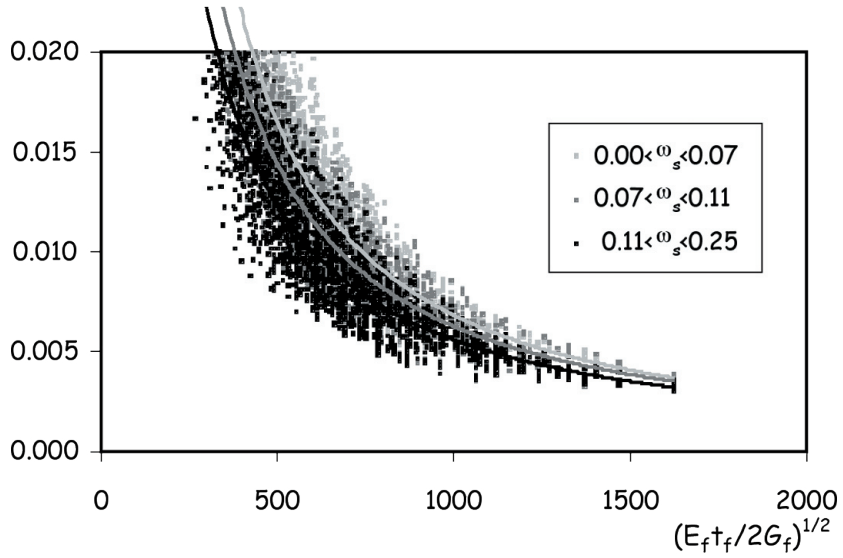

Fig. 16. Maximum FRP strain at debonding for different values of steel "mechanical ratio" ω_s.

All the cases considered in the parametric analysis refer to a simply supported beam under a uniformly distributed load, which represents one of the most common load conditions. On the contrary, the experimental results are usually obtained under concentrated loads resulting in three or four points bending schemes. Moreover, code provisions and other simplified proposals usu-

ally derive by calibrating the coefficients of simplified analytical relationships with respect to the corresponding experimental results. Nevertheless, it is interesting to underline that maximum axial strain developed in FRP at debonding is hugely affected by load conditions. Some of the beams considered in the parametric analysis of the previous paragraph have been studied even under four-point-bending conditions with a/L=1/3. Fig. 17 shows how different are the $\varepsilon_{f,max}$ values obtained under a uniformly distributed load and two concentrated forces. In particular, $\varepsilon_{f,max}$ values obtained in the case of distributed load are usually greater than those determined under concentrated loads. In fact, being intermediate debonding failure basically controlled by interface shear stresses in correspondence of yielded sections of RC beams, concentrated load schemes, characterized by uniform values of shear force, exhibit performances worse than those obtained under uniformly distributed load.

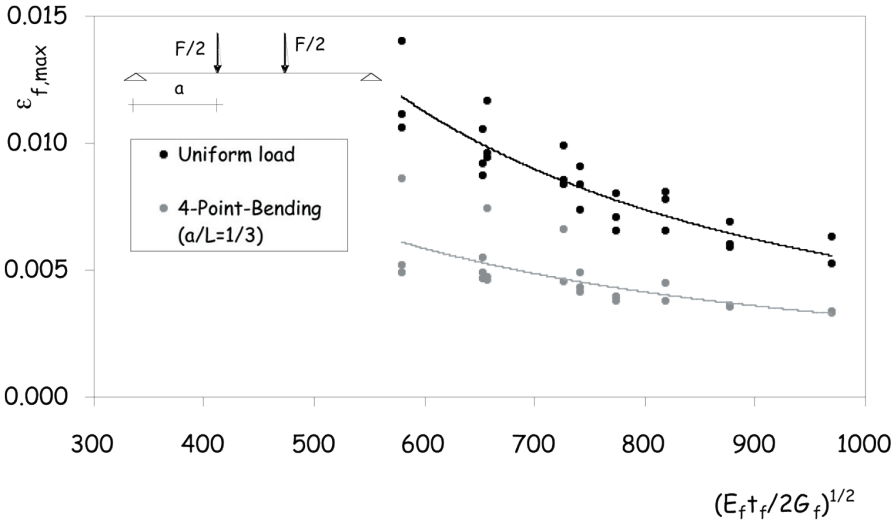

Fig. 17. Load scheme effect on FRP axial strain at debonding

5 CONCLUSIONS

A numerical model has been formulated for simulating the whole flexural behavior of FRP-strengthened RC beams. Non-linear stress-strain relationships have been considered for modeling the behavior of the structural materials and the adhesive interface. The numerical procedure carried out implementing an iterative secant algorithm to follow the various non-linear relationships introduced for simulating FRP-strengthened beam in flexure is numerically efficient. Moreover, a sensitivity analysis, usually a key test for a finite element model especially when non-linear (and softening) stress-strain relationships are considered in the analysis, has been performed; it showed that no relevant mesh-dependence exists when the discretization is refined as usual in non-linear problems.

A wide section of the present paper has been devoted to validate the mentioned model in order to assess its ability and accuracy in reproducing the experimentally observed behavior. The proposed experimental-to-numerical comparisons have shown the remarkable precision of the model in simulating the evolution of the structural behavior and predicting the failure mode.

The numerical procedure presented and validated in the paper has been utilized as a powerful tool to extend the experimental data, reaching a number of cases which is far larger than the one realizable in a laboratory for practical reasons. Consequently, the influence of the various parameters has been briefly investigated to understand their role and quantifying their importance. Some of these parameters have been already considered in various simplified proposals, while other parameters have not yet been considered and further studies are needed for quantifying its effect on debonding failure.

References

Chen J.F., Teng J.G. (2001)**:** Anchorage Strength Models for FRP and Plates Bonded to Concrete, ASCE Journal of Structural Engineering, vol. 127, No. 7, July, 784-791;

Roberts T. M. (1988): Approximate analysis of shear and normal stress concentrations in the adhesive layer of plated RC beams, The Structural Engineer, Vol. 66, No. 5, 85-94;

Malek A. M., Saadatmanesh H., Ehsani M. R. (1998), Prediction of failure load of R/C beams strengthened with FRP plate due to stress concentration at the plate end, ACI Structural Journal, Vol. 95, No. 2, , 142-152;

Holzenkaempfer (1994), Ingenieurmodelle des verbundes geklebter bewehrung fur betonbauteile, Dissertation, TU Braunschweig (in German);

Taljsten B. (1997), Strengthening of Beams by plate bonding, Journal of Materials in Civil Engineering, ASCE, 9 (4), 206-212;

Teng J.G., Chen J.F., Smith S.T., Lam L. (2002): FRP-strengthened RC Structures, J. Wiley & Sons, GB;

Task Group 9.3 (2001), Externally Bonded FRP Reinforcement for RC Structures, Technical Report Bulletin 14, fib-CEB-FIP;

ACI Committee 440.2 R-02 (2002): Guide for the Design and Construction of Externally Bonded FRP Systems for Strengthening Concrete Structures, Revised 28;

JSCE (2001): Recommendations for upgrading of concrete structures with use of continuous fiber sheets, Concrete Engineering Series 41;

CNR DT 200 – First Draft (2004): Instructions for Design, Execution and Control of Strengthening Interventions by Means of Fibre-Reinforced Composites (in Italian), Italian National Research Council;

Newmark N.M., Siess C.P., Viest I.M. (1951): Tests and Analysis of Composite Beams with Incomplete Interaction, Proc. Soc. Exp. Stress Analysis, 9, 1951, 75-92;

Faella C., Martinelli E., Nigro E. (2002a): Steel and concrete composite beams with flexible shear connection: "exact" analytical expression of the stiffness matrix and applications, Computer & Structures, Vol. 80/11, pp. 1001-1109.

Faella C., Martinelli E., Nigro E. (2002b): Aderenza tra calcestruzzo e Lamine di FRP utilizzate come placcaggio di elementi inflessi. Parte II: modelli teorici ed elaborazioni numeriche, Proceedings of the XIV Congresso C.T.E. (in Italian), Mantua (Italy), 7-8 November, 237-245;

Liu I., Oehlers D.J., Seracino R. (2004), Parametric study of intermediate crack (IC) debonding on adhesively plated beams, Proceedings of FRP Composites in Civil Engineering – CICE 2004, Adelaide (Australia), 8-10 December;

Sharma S.K., Mohamed Ali M.S., Sikdar P.K. (2004), Investigation of debonding failure in FRP plated beams, Proceedings of FRP Composites in Civil Engineering – CICE 2004, Adelaide (Australia), 8-10 December 2004;

Beber A.J. (2003), Comportamento Estrutural de Vigas de Concreto Armado Reforçadas com Compósitos de Fibra de Carbono, tese de doutorado em Engenharia Civil da Universidade Federal do Rio Grande do Sul (in portuguese);

Beber A.J., Campos Filho A., Campagnolo J.L. (1999), Flexural strengthening of R\C beams with CFRP sheets, Structural Faults + Repair-99.

Gao Bo, Kim J.K., Leung C.K.Y. (2004) , Experimental study on RC beams with FRP strips bonded with rubber modified resins Catalogo Elsevier, Composites Science and Technology 64 (2004) pp. 2257-2264, July.

Garden H.N., Quantrill R.J., Hollaway L.C., Thorne A.M., Parke G.A.R. (1998), An experimental study of the anchorage length of carbon fibre composite plate used to strengthen reinforced concrete beams, Construct Build Mater, 12, 1998.

Maalej M., Leong K.S. (2005), Effect of beam size and FRP thickness on interfacial shear stress concentration and failure of FRP strengthened beams, Catalogo Elsevier, Composites Science and Technology 65 (2005) pp. 1148-1158, January.

Pham H., Al-Mahaidi R. (2004), Prediction models for debonding failure loads of CFRP retrofit-

ted RC beams, Proceedings of FRP Composites in Civil Engineering – CICE 2004, Adelaide (Australia), 8-10 December 2004;

Shahawy, M. A.; Arockiasamy, M., Beitelman, T., Sowrirajan (1996), Reinforced concrete rectangular beams strengthened with CFRP laminates Composites Structures - Part B, 27, pp. 225-233;

Spadea G., Bencardino F., Swamy R.N. (1998), Structural behavior of composite RC beams with externally bonded CFRP, J Comps Construct, ASCE, 2(3), 1998.

Taheri F. & Shahin V & Widiarsa I. (2002), On the parameters influencing the performance of reinforced concrete beams strengthened with FRP plates, Catalogo Elsevier (Composites Structures), n°58, pp.217-226.

Teng J.G., Smith S.T., Yao J., Chen J.F. (2003), Intermediate crack-induced debonding in RC beams and slabs, Construction and Buildings Materials, 17, 2003.

Zarnic R., Gostic S., Bosiljkov V., Bokan-Bosiljkov V. (1999), Improvement of bending load-bearing capacity by externally bonded plates, Proceedings of Creating with Concrete, London, Telford, 1999.